RSC Advances

ROYAL SOCIETY OF CHEMISTRY

www.rsc.org/advances

Cite this: DOI: 10.1039/c0xx00000x

www.rsc.org/xxxxxx

ARTICLE TYPE

Ultrafine Carbamazepine nanoparticles with enhanced water solubility rate of dissolution†

Raj Kumar and Prem Felix Siril*

Received (in XXX, XXX) Xth XXXXXXXXX 20XX, Accepted Xth XXXXXXXXX 20XX

DOI: 10.1039/b000000x

Carbamazepine (CBZ) is an antiepileptic drug having poor water solubility and hence poor bioavailability. Spherical nanoparticles of CBZ with particle size below 50 nm were successfully prepared by evaporation assisted solvent-antisolvent interaction (EASAI) method. CBZ nanoparticles that are stabilized by polyvinylpyrrolidone (PVP) were also prepared by the same method. Solubility of CBZ nanoparticles and CBZ-PVP nanoparticles was 11.9 and 21.5 times higher than the raw-CBZ. In vitro dissolution studies showed that almost 100 % of the drug was released from CBZ nanoparticles and CBZ-PVP nanoparticles in less than 60 min whereas only 34 % of the drug was released from raw-CBZ even after 180 min. Effect of different experimental parameters such as concentration of drug and presence of PVP on particle size, morphology, solubility and in vitro drug release rate of CBZ was thoroughly investigated. Spherical morphology of the nanoparticles was confirmed by field emission scanning electron microscopy (FESEM) and transmission electron microcopy (TEM). FTIR spectroscopy studies revealed that there is hydrogen bonding between PVP and CBZ molecules in the CBZ-PVP nanoparticles. X-ray diffraction (XRD) pattern of CBZ-PVP nanoparticles revealed the subtle change in crystal structure of raw-CBZ. Differential scanning calorimetry (DSC) studies showed that the nanoparticles were relatively less crystalline than the raw-CBZ.

1 Introduction

CBZ (5H-dibenz(b,f)azepine-5-carboxamide) is a widely used antiepileptic agent in the therapy of psychomotor seizures and trigeminal neuralgia.[1, 2] It is generally administered orally as it is having high intestinal permeability. But, its absorption in the body is slow and irregular because it is having poor solubility in water.[3] Poor water solubility of active pharmaceutical ingredients (APIs) in general is a serious challenge in drug development. Drug molecules having high permeability and low solubility are classified as class II APIs in biopharmaceutical classification system (BCS).[4, 5] CBZ is a BCS class-II drug. A large number of drugs that are identified through molecular screening programs fall under BCS class-II.[6-8] Poor water solubility also often results in poor bioavailability and fed-fasted variations. The problem of poor solubility can be solved by reducing the particle size of drugs. Decreasing the particles size increases the surface area which enhances the solubility and dissolution rate and hence the bioavailability of BCS class-II APIs.[9-11] Formulating the drugs using surfactants, polymers, lipids and liposomes can also be used as a strategy to enhance the solubility of drugs.[12-15] Nanoformulation could be used as a strategy for the application of BCS-IV APIs (poorly soluble and impermeable) also. Nanosized particles of drugs can be produced by using a number of methods. Different techniques for the preparation of nanoparticles can be broadly classified into two categories based on the production principle; bottom up processes and top down processes. The top down methods[16, 17] are mechanical processes such as media milling,[18, 19] high pressure homogenization,[20] and microfluidization.[21, 22] Processes such as supercritical fluid (SCF) technology,[23-26] evaporative precipitation into aqueous solution (EPAS),[27, 28] emulsion solvent evaporation,[29, 30] sonoprecipitation,[31] and spray-freezing into liquid[27, 32] fall in the bottom up category.[33-35] These methods have relative advantages or shortcomings. For example, wet media milling can incorporate impurities in the resulting drug particles.[36-38] Finding a suitable solvent to dissolve the API and an antisolvent that has good miscibility with the solvent is the key challenge in the bottom up 'precipitation' processes.[38, 39]

A number of attempts on particle size reduction of CBZ are reported in the literature. However, particle size reduction into micron or sub-micron levels only could be achieved yet. Spray drying technique was applied for the preparation of CBZ loaded chitosan and hydroxypropyl methoxycellulose microspheres of particle size 1-3 μm.[40] Preparation of CBZ loaded enteric microparticles having size 3.6 – 34.8 μm was also reported[41]. Attempt to improve solubility of CBZ by preparing microstructures of ternary solid dispersion having particles size less than 142 μm was also reported.[42] Antisolvent crystallization from an organic solvent was reported to produce microparticles of size 60-100 μm.[43] Supercritical anti-solvent method was used to prepare CBZ microparticles of 200-400 μm.[44] Sub-micron sized particles of CBZ were produced using spontaneous emulsification process[45] and rapid expansion of supercritical solution (RESS) method[46]. Chitosan solid lipid nanoparticles of CBZ with particles size 158-170 nm is also reported.[47] Notably, none of the methods reported so far have not achieved less than

100 nm sized particles of CBZ. Thus, there is need to develop a suitable method for the preparation of truly nanosized CBZ particles. This is especially important because CBZ is commercially available only for oral intake till date. Nanosized formulation of CBZ can have better solubility in water and they can be developed for parenteral drug administration also. Preparation of CBZ nanoparticles with average particles size well below 100 nm is reported in the present paper.

If a suitable solvent-antisolvent pair can be identified, the antisolvent precipitation process is a simple and effective technique to produce nanosized particles. For BCS class-II APIs, it is ideal to have water as the antisolvent. Instantaneous precipitation occurs by a rapid desolvation of the hydrophobic active ingredient in the antisolvent medium. The rate of nucleation of this process can be further enhanced by heating the anti-solvent to high temperatures, which is used in EPAS.[27] Here we report the preparation of CBZ nanoparticles with particles size below 100 nm and spherical morphology using EASAI method.

Increase in solubility and bioavailability of poorly water soluble drugs can be achieved by simple nanonization alone. However, a combination of nanonization and polymer encapsulation is expected to result in further enhancement of solubility. Mostly water soluble polymers are used in such formulations. Thus CBZ-PVP nanoparticles were also prepared in the present study using the EASAI method. PVP is a food and drug administration (FDA) approved inactive ingredient and is widely used as an excipient in drug formulations because it is non-toxic, chemically inert, non-ionic, and colorless.[48] One of the outstanding properties of the soluble PVP products is their universal solubility in hydrophylic and hydrophobic solvents.[48-50]

2 Materials and methods

2.1 Materials

CBZ, acetone and PVP K 30 (avg. M.W. 40,000) were purchased from Sigma Aldrich and were used as received. PBS buffer of pH 7.4 was purchased from Merck. Ultra-pure water (18.2 MΩ-cm) from double stage water purifier (ELGA PURELAB Option-R7) was used throughout. HPLC micro syringe (500 µl) was from Hamilton, USA. Needle of the syringe had a tapered nozzle having inner diameter of 0.15 mm, outer diameter of 0.72 mm and length of 2 inches. Syringe filter of 0.22 µm, 0.45 µm and Whatman, Anodisc 25, filter of 20 nm pore size were from Millipore, USA.

2.2 Preparation of CBZ nanoparticles

Accurately weighed CBZ was dissolved in acetone to make a solution of 25 mM concentration. This stock solution was diluted to get 5 mM solution for some experiments. The CBZ solution was always filtered before injection using a syringe filter of pore size 0.22 µm to ensure that no particle was present in it. 25 ml of water was taken in a 100 ml conical flask and was heated to 70 °C. 500 µl of CBZ solution was quickly injected into water using a HPLC microsyringe under stirring at constant temperature of 70 °C to obtain CBZ nanoparticles. Stirring was continued for few minutes after injection to complete the mixing. The prepared particles were collected on a membrane having pore size of 20 nm by vacuum filtration. The samples were dried by keeping in a hot air oven at 40 °C for 12 h. CBZ solution was injected to aqueous solution containing PVP for the preparation of CBZ-PVP nanoparticles. The concentration of stabilizer was optimized by changing the concentration of PVP systematically from 0.1% (w/v) to 0.4% (w/v). The ratio of solvent to antisolvent was kept the same (1:50) and the temperature of antisolvent during injection was maintained at 70 °C for all experiments. All experiments were done for two different drug concentrations (5 mM and 25 mM). Synthesis at each condition was done in triplicate to check the reproducibility.

2.3 Particle size measurement

Immediately after the precipitation of nanoparticles, the primary characterization of the particle size (z-average diameter, d / nm) and zeta potential measurement was done using DLS method (Zetasizer Nano ZS, Malvern Instrument Ltd., UK) at 25 °C. The instrument contains a 4 mW He–Ne laser operating at a wavelength of 633 nm and incorporates noninvasive backscatter optics (NIBS). The measurements were made at a detection angle of 173°. The sample containing polystyrene cuvette was placed in the temperature controlled chamber to maintain constant temperature (25 °C). Polydispersity index (Pdi) was also recorded, which is a measure of particle size distribution. Pdi is a dimensionless parameter calculated from a simple two parameter fit to the correlation data in DLS. Zeta potential of nanoparticles was determined by measuring the electrophoretic mobility of nanoparticles using Zeta cell at 25 °C. All the measurements were made in triplicate and mean values with standard deviations are being reported.

2.4 FESEM

Particle size and morphology of samples was also observed using an FESEM (Carl Zeiss model Supra 55VP). The suspension of CBZ nanoparticles in water was drop coated on clean glass slides and dried. The dried glass slide was transferred onto carbon tape applied on a clean SEM stub. Samples were subsequently sputter-coated with gold at 20 mA for 180 s before the FESEM observations. Particles size (d / nm) of at least 300 particles from many images of different regions were measured using Image J software and mean particle size was calculated.

2.5 Transmission electron microscopy

The samples were negatively stained before the TEM imaging of prepared CBZ and CBZ-PVP nanoparticles. The aqueous suspensions of the samples were drop coated on TEM grids and incubated for 180 s. The samples were then stained using 2% (w/v) aqueous solution of phosphotungstic acid (PTA). Excess PTA was removed by washing with ultra-pure water. Imaging was done using TEM (FEI, Tecnai G^2, S-Twin) at 200 kV.

2.6 FTIR spectroscopy

FTIR spectroscopy was performed using the Perkin Elmer FTIR emission spectrometer (Spectrum Two). The FTIR spectrum of CBZ nanoparticles was recorded from 4000 cm^{-1} to 600 cm^{-1} frequency range with a resolution of 4 cm^{-1} and 8 scans. The samples were properly grounded with KBr powder and then

pressed to obtain a suitably sized pellet for FTIR spectrum measurement. Pure KBr pellet was used for background correction.

2.7 Powder X-ray diffraction (XRD)

XRD was performed on a Smart Lab X-Ray Diffractometer (Rigaku, Japan) using Cu Kα radiation as x-ray source (λ = 0.15418 nm) at room temperature. The voltage and current applied were 45 kV and 100 mA respectively. Samples were placed in a glass sample holder and scanned from 2θ - 10° to 70° at a scan rate of 2 degrees per min with a step size of 0.02°.

2.8 TGA-DSC

TGA-DSC analyses were carried out by using a Netzsch STA 449 F1 Jupiter instrument. Small amount of the sample (2-3 mg) was kept in a standard alumina crucible with an alumina lid with a pin hole at the middle. An empty crucible was used as reference. The samples were heated from room temperature to 300 °C at a heating rate of 10 °C/min under nitrogen atmosphere with a flow rate of 60 ml min^{-1}.

2.9 Solubility measurements

Solubility of the samples in water was measured according to the method reported previously.[46] An excess amount of each sample (30 mg) was weighed accurately and added to water (25 ml) in a 100 ml conical flask. The samples were magnetically stirred at 100 rpm inside a thermostatic water bath that was maintained at 37±1 °C for 24 h. After 24 h the suspensions were filtered using a syringe filter having pore size of 0.02 µm to remove undissolved particles. The filtrate was diluted 10 fold by adding water and absorbance was determined using a Shimadzu UV-Vis spectrophotometer. Optical density at characteristic absorption maximum of CBZ at (λ_{max} 287 nm) was used to compare the solubility of CBZ nanoparticles and CBZ-PVP with raw CBZ.

2.10 In-vitro drug release profile studies

In vitro drug release test was performed with a USP microprocessor dissolution apparatus, model 1912, (Electronics India, India) using a rotating basket method. Dissolution rate of CBZ samples (10 mg) was tested in 900 ml of phosphate buffer of pH 7.4. The speed of rotation was set at 50 rpm and the temperature of the dissolution medium was maintained at 37±1 °C. Aliquots (2 ml) were withdrawn at predetermined time intervals (0, 5, 10, 15, 20, 25, 30, 45, 60, 120 and 180 min). The sink was replenished with 2 ml phosphate buffer immediately after withdrawing each aliquot to maintain a constant volume. UV-visible absorption spectrum of each aliquot was recorded after filtering the samples through a Whatman Anodisc 25 filter of pore size 0.02 µm. Optical density at characteristic absorption maximum of CBZ (λ_{max} - 287 nm) was used to quantify the amount of dissolved CBZ.

3 Results and discussion

Injection of CBZ solution into water under stirring leads to the formation of nanoparticles immediately as we detected nanosized particles in DLS within few minutes after the injection. The stirring was continued up to few minutes after injection to complete the mixing which is reported to yield smaller particles size with narrow size distribution.[35] Though, antisolvent precipitation is a very simple method, a number of experimental factors such as temperature of antisolvent, concentration of the solution and ratio of solvent to antisolvent are known to influence the particle size.[35] Most of the parameters that are relevant to our experiments were optimized in a previous study on the preparation of RDX nanoparticles and we used similar experimental conditions in the present study.[51] However, the effect of concentration of solution and the presence of PVP on particles size was studied and the results are presented in the following sections.

3.1 Optimization of stabilizer concentration

PVP was used as a stabilizer and the concentration of the stabilizer was optimized to prepare nanoparticles with smaller particle size. Experimental conditions and the mean particles size from DLS with standard deviation are reported in Table 1. It is evident from Table 1 that the particles size was lowest when the PVP concentration was 0.2% (w/v). Thus, 0.2 % (w/v) was found to be the optimum concentration. The CBZ-PVP nanoparticles prepared with the optimized PVP concentration was further characterized thoroughly.

Table 1. Effect of change in concentration of PVP on particle size of CBZ-PVP nanoparticles measured using DLS.

S. No	PVP / % (w/v)	Antisolvent vol./ ml	Drug / mM	Volume of solvent / µl	Particles size (d) / nm
1	0.1	25	5	500	369±60
2	0.2	25	5	500	250±13
3	0.4	25	5	500	542±217
4	0.1	25	25	500	650±21
5	0.2	25	25	500	295±41
6	0.4	25	25	500	971±19

3.2 Effect of drug concentration and presence of PVP on particles size

The effect of concentration of the CBZ solution on the size of particles at constant temperature was also studied. The particle size as per DLS measurements and from FESEM imaging is reported in Table 2. DLS data is shown in Fig. S1 (ESI†) and some representative FESEM images are shown in electronic supporting information (S2†, S3†, S4† and S5†). From the data presented in Table 2 it is apparent that the particle size increases as the concentration of CBZ increases. A similar trend of increase in particles size with increase in concentration was observed in our previous studies also.[51] The increase in particle size with the increase in concentration of the solution may be because there is enough supply of the precursor to sustain the growth of nuclei long enough so that the nuclei grow into relatively bigger

particles. However, the particle size was in nanometer length scale even at the highest concentration tested, i.e. 25 mM.

Table 2. Effect of drug concentration on particle size and zeta potential (ZP) of CBZ nanoparticles and CBZ-PVP nanoparticles.

S. No.	Sample	Particles size (d)/ nm		PDI	ZP / mV
		DLS	SEM		
1	5 mM CBZ	221±12	18±8	0.28±0.02	-8.8 ±1.4
2	5 mM CBZ-PVP	250±13	33±9	0.30±0.02	-4.0 ±0.4
3	25 mM CBZ	269±26	38±13	0.36±0.10	-17.0 ±2.0
4	25 mM CBZ-PVP	295±41	47±18	0.36±0.03	-4.5 ±1.3

It can also be concluded from the data presented in Table 2 that the particle size increases slightly when PVP was used as a stabilizer. This shows that PVP gets adsorbed on the CBZ nanoparticles once they are formed. The zeta potential of CBZ and CBZ-PVP nanoparticles are reported in Table 2. The zeta potential of CBZ nanoparticles becomes less negative when they are prepared in presence of PVP. This also shows that the polymer is present on the surface of the nanoparticles.

The mean particle size (z-average) calculated from DLS was found to be significantly higher than the mean diameter calculated from FESEM images. This may be due to a number of reasons. Firstly, DLS measures the hydrodynamic diameter of particles which is always higher than the actual particle size. Secondly presence of a small fraction of large sized particles can result in a higher z-average value in particle size measurement using DLS. Additionally, DLS cannot differentiate between individual particles and aggregates. Hence, the presence of even a small amount of aggregates will result in higher z-average particle size in DLS. On the contrary, FESEM is a direct method for viewing the particles and the particle size that is estimated from FESEM is hence more reliable. We have estimated average particle size from different images that were captured from different region on the sample and hence the particle size from FESEM imaging must be more reliable.

3.3 Morphology of the nanoparticles

Spherical nanoparticles with very small particle size were seen in FESEM images (ESI Fig. S2†, S3†, S4† and S5†). Aggregation of the particles was not observed even in absence of PVP. The TEM images of negatively stained CBZ nanoparticles and CBZ-PVP nanoparticles are shown in Figure 1. The TEM images also confirmed the spherical shape of the nanoparticles. The CBZ nanoparticles did not have a smooth surface. A dark core surrounded by light corona was observed for most of the particles (Fig. S6, ESI†). This may be due to the amorphous nature of the particle surface. Population of the particles on the TEM grids was relatively low, when compared to what we observed in FESEM images. This is partly because the difference in the method of sample preparation that was used in TEM and FESEM. In FESEM, the aqueous suspension of the samples was dropped on glass slides and was allowed to dry. This leads to the deposition of all particles on the glass slide. However, a large number of very small particles do not to get settled down under gravity during the incubation period of 180 s on TEM grids. Moreover, a number of particles get washed away during the washing cycle after deposition of PTA. Thus, relatively bigger particles only get deposited and remains on the TEM grids.

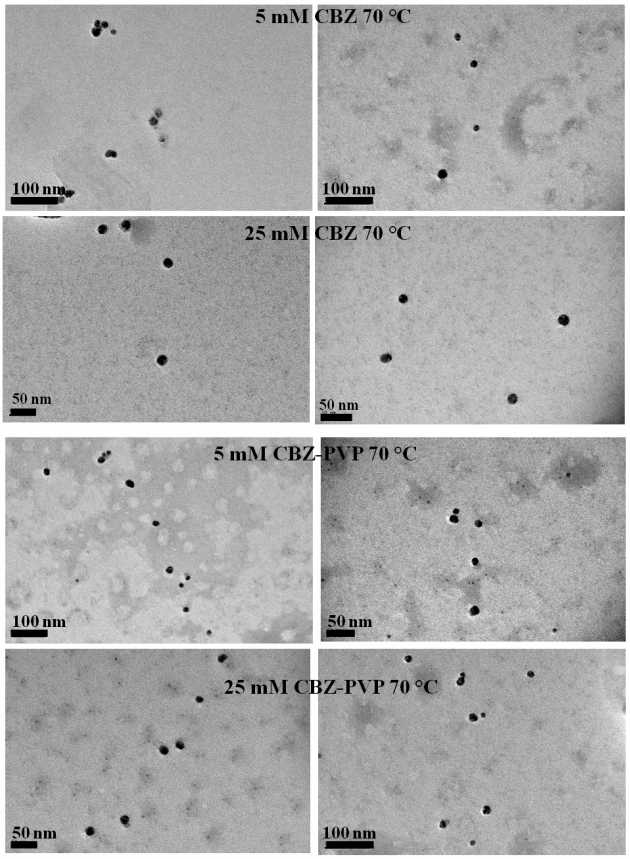

Fig. 1. TEM images of CBZ nanoparticles and CBZ-PVP nanoparticles prepared from 5 mM and 25 mM CBZ solutions at 70 °C.

3.4 Chemical composition of the CBZ nanoparticles and compatibility with PVP.

FTIR spectroscopy was used to compare the chemical composition of raw-CBZ with the bare CBZ nanoparticles and CBZ-PVP nanoparticles. The FTIR spectra are shown in Figure 3. It was observed that the raw-CBZ and the prepared CBZ nanoparticles showed similar IR bands. The major bands at 3465 cm^{-1} and 3159 cm^{-1} (–NH), 1687 cm^{-1} (-CO-R), 1605 cm^{-1} (-C=C-) and at 1488 cm^{-1} ($–NH_2$) showed that there was no chemical modification of CBZ during the preparation of the nanoparticles. The CBZ-PVP nanoparticles also showed similar FTIR spectrum to raw-CBZ. However, the IR band at 1687 cm^{-1} of raw-CBZ was

shifted to 1678 cm^{-1} in CBZ-PVP. The shifting of the peak is visible in the FTIR spectra of the wavenumber region between 1000 cm^{-1} to 2000 cm^{-1} that is given in the electronic supporting information (Figure S7, ESI†). Such a shifting indicates the formation of hydrogen bonding between carbonyl group of CBZ and PVP.[42, 52]

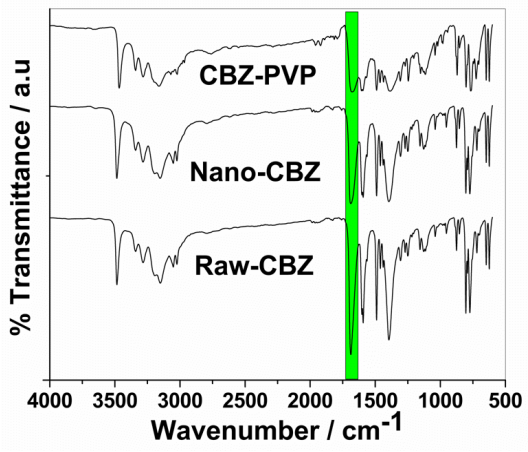

Fig. 2. FTIR spectra of raw-CBZ, nano-CBZ and CBZ-PVP.

3.5 Crystal structure

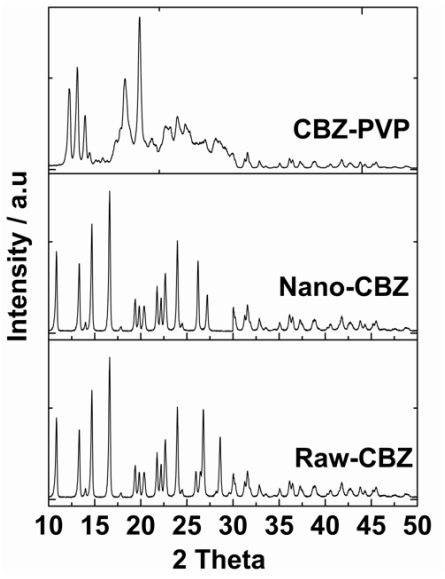

Fig. 3. XRD spectra of raw-CBZ, nano-CBZ and CBZ-PVP.

XRD patterns of the nano-CBZ and CBZ-PVP nanoparticles were recorded and compared with the XRD pattern of raw-CBZ to ascertain the crystalline nature of the nanoformulated CBZ. The XRD patterns are shown in Figure 4. All the characteristic peaks of raw-CBZ matched well with the peaks of CBZ nanoparticles. The raw-CBZ was in the β-form or form-III (JCPDF Card number 51-2106, p-monoclinic cell, a = 7.537 Å, b = 11.156 Å, c = 13.912 Å).[53] The CBZ nanoparticles also precipitated in the β-polymorphic form as it is the thermodynamically most stable form.[53] However, the XRD pattern of CBZ-PVP nanoparticles was significantly different from the XRD pattern of raw-CBZ. A number of peaks disappeared completely and new broad peaks observed because of the presence of PVP and H-bonding between CBZ and PVP.[54, 55] The subtle changes in the diffraction patterns may be due to the inclusion of PVP in the crystal lattice and change in crystallinity as well as particle size.

3.6 Thermal characteristics

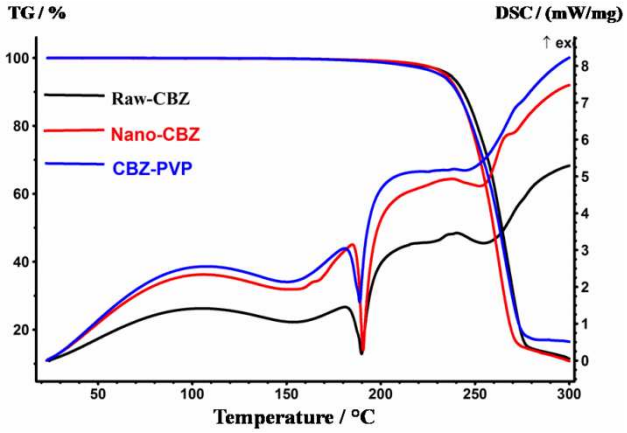

Fig. 4. TGA-DSC thermal curves of raw-CBZ, nano-CBZ and CBZ-PVP.

An overlay of TGA-DSC thermal curves of raw CBZ along with CBZ and CBZ-PVP nanoparticles are shown in Figure 5. The corresponding phenomenological data is summarized in Table 3. The DSC thermal curves of raw-CBZ, nano-CBZ and CBZ-PVP nanoparticles showed endothermic peaks at about 190.8 °C, 189.8 °C and 188.7 °C respectively. The endothermic peak around this temperature corresponds to the melting of form-I of CBZ.[42,45] The melting point of raw-CBZ was 187.5 °C. Melting point of CBZ nanoparticles was 186.4 °C and for CBZ-PVP nanoparticles this was 183.6 °C. Melting of form-III appears usually as an endotherm in DSC thermal curved of CBZ at ~175 ^{0}C followed by an exotherm corresponding to crystallization into form-I. The form-I melts at around 190 ^{0}C subsequently.[42,45, 56] All the three thermal events were observed in the thermal curves for nano-CBZ only. For raw-CBZ and the CBZ-PVP, melting of form-III and crystallization into form-I got unregistered due to the low sample mass that was used to record the TGA-DSC when compared to nano-CBZ. Relative crystallinity of the samples was also calculated from the DSC data by assuming that the raw-CBZ was 100% crystalline. The data is reported in Table 3. It was found by comparing the enthalpy of melting of the samples that the nano-CBZ and CBZ-PVP were much less crystalline compared to raw-CBZ. Mass loss (% w/w) for all the samples at 300 °C is given in Table 3. Mass loss for nano-CBZ was similar to raw-CBZ. However, mass loss for CBZ-PVP was relatively less at 300 °C compared to raw-CBZ. This may be due to the presence of residual PVP being present along with the residues from the thermolysis of CBZ. PVP is a thermally stable polymer and it does not decompose at temperatures below 300 ^{0}C in nitrogen atmosphere.[57] By comparing the % mass loss of the three samples, we can conclude that there was ~ 5% (w/w) of PVP was present in CBZ-PVP nanoparticles.

Table 3. Summery of TGA-DSC data of raw-CBZ, nano-CBZ and CBZ-PVP.

S. No.	Sample	T(Onset) / °C	T(Peak) / °C	ΔH / (J/g)	Crystallinity	%Mass loss
1	Raw-CBZ	187.5	190.8	-88.5	100.0	88.5
2	Nano-CBZ	186.4	189.8	-53.2	60.1	89.2
3	CBZ-PVP	183.6	188.7	-48.6	55.0	83.5

3.7 Solubility measurement

Relative solubility of CBZ nanoparticles and CBZ-PVP nanoparticles were tested against raw-CBZ. Results revealed that there is significant increase in solubility for the nanoparticles compared to raw-CBZ. CBZ nanoparticles were found to be 11.9 times more soluble than raw-CBZ. CBZ-PVP nanoparticles have 21.5 times more solubility than raw-CBZ. Results revealed that PVP influence the solubility significantly. PVP is a water soluble polymer and it enhances the solubility due to its hydrophilic nature. Additionally, CBZ nanoparticles and CBZ-PVP nanoparticles were found to be significantly less crystalline than raw-CBZ. This also contributes to the enhanced solubility of the drug nanoparticles.

3.8 In vitro dissolution studies

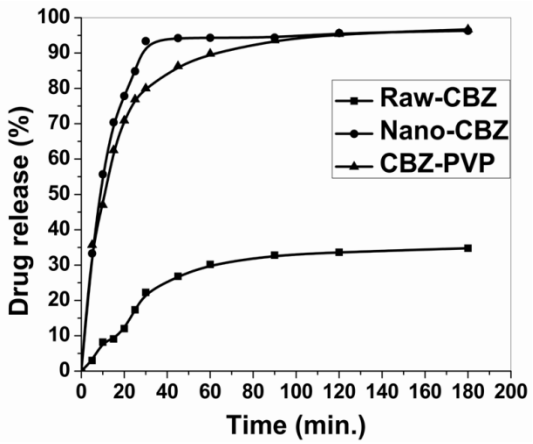

Fig. 5. In-vitro dissolution profile of raw-CBZ, nano-CBZ and CBZ-PVP.

The in-vitro dissolution profiles for all samples are shown in Figure 6. The results revealed a significant increase in the drug release profiles due to nanonization. 95 % of the drug molecules from bare CBZ nanoparticles and 96 % of the drug molecules from CBZ-PVP nanoparticles were released within 60 min whereas only 34 % of the drug was released from raw-CBZ even after 180 min. Infact, more than 50% of the drug molecules were released into water in less than 10 min for nano-CBZ and CBZ-PVP nanoparticles. Such drastic difference in rate of dissolution between raw-CBZ and the nano-sized CBZ is due to the decrease in particles size and increase in surface area of CBZ nanoparticles. Increased presence of amorphous CBZ in the nanonized samples may also contribute to the enhancement in dissolution rate. The rate of drug release from CBZ-PVP was slightly slower than the drug release rate from nano-CBZ after the release of 50 % of the drug. This may be due to the interaction between the drug and PVP molecules. The interaction may be limiting the formation of dihydrate form of CBZ which has higher solubility and dissolution rate than the anhydrous form of CBZ. Dihydrates are formed usually when the anhydrous CBZ molecules comes into contact with water.[56] This opens up a possibility to modulate the release profile of CBZ nanoparticles using PVP.

4 Conclusions

CBZ nanoparticles and CBZ-PVP nanoparticles with spherical morphology was successfully prepared by EASAI method. Size reduction and presence of PVP has a profound effect on the crystallinity, solubility and drug release profile of CBZ. Solubility can be enhanced many folds and nearly 100% release of CBZ molecules can be achieved by nanoformulation using EASAI method. However, the possibility of recrystallization of amorphous CBZ in the nanonized samples may lower the solubility on storage and this aspect has to be studied in detail.

Acknowledgement

Thanks are due to Advanced Materials Research Centre, IIT Mandi for providing laboratory facilities. Financial assistance from ARMREB (DRDO), IIT Mandi and UGC (SRF) is gratefully acknowledged.

Notes and references

[a] *School of Basic Sciences, Indian Institute of Technology Mandi, Mandi-175005, Himachal Pradesh, India. Fax: +91-1905-237942; Tel: +91-1905300040; E-mail: prem@iitmandi.ac.in*

† Electronic Supplementary Information (ESI) available: DLS data of prepared CBZ nanopartcles at different experimental condition (ESI Fig.S1†) and FESEM images of CBZ nanoparticles prepared at different experimental conditions (ESI Fig.S2†, Fig.S3†, Fig S4† and Fig S5†) TEM images of nano-CBZ and CBZ-PVP (ESI Fig.S6†) and FTIR spectra in the range 1000 cm^{-1} to 2000 cm^{-1} (ESI Fig. S6†). See DOI: 10.1039/b000000x/

1. J. Graham and K. Zilkha, *Br. Med. J.*, 1966, **1**, 210.
2. J. J. Cereghino, J. T. Brock, J. C. Van Meter, J. K. Penry, L. D. Smith and B. G. White, *Neurology*, 1974, **24**, 401-401.
3. M. Lindenberg, S. Kopp and J. B. Dressman, *Eur. J. Pharm. Biopharm.*, 2004, **58**, 265-278.
4. R. Löbenberg and G. L. Amidon, *Eur. J. Pharm. Biopharm.*, 2000, **50**, 3-12.
5. T. Takagi, C. Ramachandran, M. Bermejo, S. Yamashita, L. X. Yu and G. L. Amidon, *Mol. Pharm.*, 2006, **3**, 631-643.
6. H. Chen, C. Khemtong, X. Yang, X. Chang and J. Gao, *Drug Discovery Today*, 2011, **16**, 354-360.
7. N. A. Kasim, M. Whitehouse, C. Ramachandran, M. Bermejo, H. Lennernäs, A. S. Hussain, H. E. Junginger, S. A. Stavchansky, K. K. Midha and V. P. Shah, *Mol. Pharm.*, 2004, **1**, 85-96.
8. E. M. Merisko-Liversidge and G. G. Liversidge, *Toxicol. Pathol.*, 2008, **36**, 43-48.

9. J.-i. Jinno, N. Kamada, M. Miyake, K. Yamada, T. Mukai, M. Odomi, H. Toguchi, G. G. Liversidge, K. Higaki and T. Kimura, *J. Control. Release*, 2006, **111**, 56-64.
10. G. G. Liversidge and P. Conzentino, *Int. J. Pharm.*, 1995, **125**, 309-313.
11. G. G. Liversidge and K. C. Cundy, *Int. J. Pharm.*, 1995, 125, 91-97.
12. P. P. Constantinides, *Pharm. Res.*, 1995, **12**, 1561-1572.
13. A. J. Humberstone and W. N. Charman, *Adv. Drug Del. Rev.*, 1997, **25**, 103-128.
14. M. Sugimoto, T. Okagaki, S. Narisawa, Y. Koida and K. Nakajima, *Int. J. Pharm.*, 1998, **160**, 11-19.
15. S. Wong, I. Kellaway and S. Murdan, *Int. J. Pharm.*, 2006, **317**, 61-68.
16. T. J. Merkel, K. P. Herlihy, J. Nunes, R. M. Orgel, J. P. Rolland and J. M. DeSimone, *Langmuir*, 2009, **26**, 13086-13096.
17. B. Van Eerdenbrugh, G. Van den Mooter and P. Augustijns, *Int. J. Pharm.*, 2008, **364**, 64-75.
18. E. Merisko-Liversidge and G. G. Liversidge, *Adv. Drug Del. Rev.*, 2011, **63**, 427-440.
19. S. K. Singh, K. Srinivasan, K. Gowthamarajan, D. S. Singare, D. Prakash and N. B. Gaikwad, *Eur. J. Pharm. Biopharm.*, 2011, **78**, 441-446.
20. C. M. Keck and R. H. Müller, *Eur. J. Pharm. Biopharm.*, 2006, **62**, 3-16.
21. J. H. Jung, T. J. Park, S. Y. Lee and T. S. Seo, *Angew. Chem.*, 2012, **124**, 5732-5735.
22. L. Capretto, D. Carugo, S. Mazzitelli, C. Nastruzzi and X. Zhang, *Adv. Drug Del. Rev.*, 2013, **65**, 1496-1532.
23. J. Jung and M. Perrut, *J. Supercrit. Fluids*, 2001, **20**, 179-219.
24. Y. Komai, H. Kasai, H. Hirakoso, Y. Hakuta, H. Katagi, S. Okada, H. Oikawa, T. Adschiri, H. Inomata and K. Arai, *JaJAP*, 1999, **38**, L81.
25. B. Subramaniam, R. A. Rajewski and K. Snavely, *J. Pharm. Sci.*, 1997, **86**, 885-890.
26. E. Reverchon, *J. Supercrit. Fluids*, 1999, **15**, 1-21.
27. J. M. Vaughn, X. Gao, M.-J. Yacaman, K. P. Johnston and R. O. Williams III, *Eur. J. Pharm. Biopharm.*, 2005, **60**, 81-89.
28. S. R. Dharmalingam, K. Chidambaram and S. Ramamurthy, *Dig. J. Nanometer. Bios*, 2013, **8**.
29. B. Kim, S. Hwang, J. Park and H. Park, *J. Microencap.* 2002, 19, 811-822.
30. I. D. Rosca, F. Watari and M. Uo, *J. Control. Release*, 2004, **99**, 271-280.
31. A. Amperiadou and M. Georgarakis, *Int. J. Pharm.*, 1995, **115**, 1-8.
32. A. Paudel, Z. A. Worku, J. Meeus, S. Guns and G. Van den Mooter, *Int. J. Pharm.*, 2013, **453**, 253-284.
33. H. S. Ali, P. York and N. Blagden, *Int. J. Pharm.*, 2009, **375**, 107-113.
34. H.-K. Chan and P. C. L. Kwok, *Adv. Drug Del. Rev.*, 2011, **63**, 406-416.
35. B. Sinha, R. H. Müller and J. P. Möschwitzer, *Int. J. Pharm.*, 2013, **453**, 126-141.
36. D. Horn and J. Rieger, *Angew. Chem. Int. Ed.*, 2001, **40**, 4330-4361.
37. M. Juhnke, D. Märtin and E. John, *Eur. J. Pharm. Biopharm.*, 2012, **81**, 214-222.
38. A. A. Thorat and S. V. Dalvi, *Chem. Eng. J.*, 2012, **181**, 1-34.
39. H. Kasai, T. Murakami, Y. Ikuta, Y. Koseki, K. Baba, H. Oikawa, H. Nakanishi, M. Okada, M. Shoji and M. Ueda, *Angew. Chem. Int. Ed.*, 2012, **51**, 10315-10318.
40. J. Filipović-Grčić, B. Perissutti, M. Moneghini, D. Voinovich, A. Martinac and I. Jalšenjak, *J. Pharm. Pharmacol.*, 2003, **55**, 921-931.
41. W. Dong, P. Maincent and R. Bodmeier, *Int. J. Pharm.*, 2007, **331**, 84-92.
42. R. M. Martins, S. Siqueira, L. A. Tacon and L. A. Freitas, *Powder Technol.*, 2012, **215**, 156-165.
43. M.-W. Park and S.-D. Yeo, *Chem. Eng. Res. Des.*, 2012, **90**, 2202-2208.
44. D. Meng, J. Falconer, K. Krauel-Goellner, J. J. Chen, M. Farid and R. G. Alany, *AAPS PharmSciTech*, 2008, **9**, 944-952.
45. R. G. Kelmann, G. Kuminek, H. F. Teixeira and L. S. Koester, *Int. J. Pharm.*, 2007, **342**, 231-239.
46. D. Bolten and M. Türk, *J. Supercrit. Fluids*, 2012, **62**, 32-40.
47. R. Nair, A. C. Kumar, V. K. Priya, C. M. Yadav and P. Y. Raju, *Lipids in Health and Disease*, 2012, **11**, 1-8.
48. D. Sharma, M. Soni, S. Kumar and G. Gupta, *Res. J. Pharm. Technol.* 2009, 2, 220-224
49. V. G. Kadajji and G. V. Betageri, *Polymers*, 2011, 3, 1972-2009.
50. B.-J. Lee, S.-G. Ryu and J.-H. Cui, *Int. J. Pharm.*, 1999, 188, 71-80.
51. R. Kumar, P. F. Siril and P. Soni, *Propellants, Explos., Pyrotechnics*, 2014. **39**, 383-389.
52. R. Chadha, V. Kapoor and A. Kumar, *J. Sci. Ind. Res.*, 2006, 65, 459.
53. A. Kogan, I. Popov, V. Uvarov, S. Cohen, A. Aserin and N. Garti, *J. Dispers. Sci. Technol.*, 2007, **28**, 1008-1019.
54. B. C. Hancock and M. Parks, *Pharm. Res.*, 2000, **17**, 397-404.
55. P. Gupta, V. K. Kakumanu and A. K. Bansal, *Pharm. Res.*, 2004, **21**, 1762-1769.
56. R. Nair, S. Gonen, S. W. Hoag, *Int. J. Pharm,* 2002, **240**, 11-22.
57. C. Peniche, D. Zaldivar, M. Pazos, S. Paz, A. Bulay, J. S. Roman, *J. of Appl. Polym. Sci*., 1993, **50**, 485-493.